Bioorganic Chemistry 153 (2024) 107959

Contents lists available at ScienceDirect

Bioorganic Chemistry

journal homepage: www.elsevier.com/locate/bioorg

Synthesis and biological evaluation of a new class of azole urea compounds as Akt inhibitors with promising anticancer activity in pancreatic cancer models

Camilla Pecoraro [a], Fabio Scianò [a,b], Daniela Carbone [a], Geng Xu [b], Juan Deng [b], Stella Cascioferro [a,*], Elisa Giovannetti [b,c,*], Patrizia Diana [a], Barbara Parrino [a]

[a] Department of Biological, Chemical, and Pharmaceutical Sciences and Technologies (STEBICEF), University of Palermo, Via Archirafi 32, 90123 Palermo, Italy
[b] Department of Medical Oncology, Cancer Center Amsterdam, Amsterdam UMC, VU University, Amsterdam 1081 HV, The Netherlands
[c] Cancer Pharmacology Laboratory, Fondazione Pisana per la Scienza, Via Ferruccio Giovannini 13, 56017 Pisa, Italy

ARTICLE INFO

Keywords:
Pancreatic ductal adenocarcinoma
1,2,3-Triazole urea compounds
Akt inhibitors
Anti-migratory activity
3D spheroid model

ABSTRACT

The PI3K/Akt pathway is crucial in numerous cellular functions such as cell growth, survival proliferation and movement in both normal and cancer cells. It plays also a key role in epithelial-mesenchymal transitions and angiogenesis during the tumorigenesis processes. Since many transformative events in cancer are driven by increased PI3K/Akt pathway signaling, Akt is considered a valuable target for developing new therapies against various tumor types, including pancreatic cancer. This is because the PI3K/AKT/mTOR pathway is a key downstream effector of RAS, and RAS activation is the most prominent genetic alteration in pancreatic cancer. Herein we report the synthesis and the biological evaluation of a new series of azole urea compounds that exhibited promising antiproliferative and antimigratory activities against pancreatic cancer cells through an Akt inhibition mechanism. These effects were demonstrated using a variety of assays, including Sulforhodamine B, cell-cycle, wound-healing, and kinase activity, apotposis and ELISA assays. Additionally, the anticancer properties of the most active compound in the series were confirmed in the 3D spheroid model of PATU-T cells.

1. Introduction

Protein kinase B (PKB), is a serine/threonine kinase that plays key roles in multiple cellular processes involved in cancer occurrence and development, such as cell proliferation, apoptosis, glucose metabolism, angiogenesis, and cell migration [1,2]. PKB, also known as Akt (AKR mouse strain that develops spontaneous thymic lymphomas), exists in three isoforms encoded by different genes: Akt1, Akt2, and Akt3 [3]. Structurally all the three isoforms show three common regions: (i) an amino terminal pleckstrin homology (PH) domain involved in the interaction with membrane phospholipids such as phosphatidylinositol-3,4,5-triphosphate (PIP3) and phosphatidylinositol-4,5-bisphosphate (PIP2); (ii) a central kinase domain containing the regulatory residue, Thr308, essential for the Akt activation; and (iii) a carboxyl-terminal regulatory domain which includes a hydrophobic region of 40 amino acids comprised of the serine regulatory residue (Ser473) [4].

Akt's activation consists of two crucial steps: (i) translocation to the plasma membrane starting with the interaction of the PH domain with PIP3 and (ii) phosphorylation at the Thr308 and Ser473 residues [5]. Once phosphorylated (pAkt), pAkt is involved in the deregulation of cellular processes such as proliferation, apoptosis, and cell motility by inducing signaling pathways that disrupt normal regulatory mechanisms, leading to the activation of the mammalian target of rapamycin (mTOR) [6].

Despite the three Akt isoforms are structurally very similar, they have different physiological functions, properties and expression patterns [7]. Akt1 is essential for cell survival, Akt2 plays a key role in glucose homeostasis, while Akt3 is involved in brain development [8]. Apart from its crucial role in normal cellular physiology, numerous studies have demonstrated the activation and overexpression of the Akt

Abbreviations: Akt, AKR mouse strain that develops spontaneous thymic lymphomas; DCM, dichloromethane; DMAP, 4-dimethylaminopyridine; FACS, Fluorescence Activated Cell Sorting; mTOR, mechanistic target of rapamycin; PDAC, pancreatic ductal adenocarcinoma; PH, pleckstrin homology; PI, propidium iodide; PIP3, phosphatidylinositol-3,4,5-triphosphate PKB, Protein kinase B; PIP2, phosphatidylinositol 4,5-bisphosphate; SRB, Sulforhodamine B; THF, tetrahydrofuran.

* Corresponding authors.
E-mail addresses: stellamaria.cascioferro@unipa.it (S. Cascioferro), elisa.giovannetti@gmail.com (E. Giovannetti).

https://doi.org/10.1016/j.bioorg.2024.107959
Received 27 September 2024; Received in revised form 4 November 2024; Accepted 11 November 2024
Available online 15 November 2024

signaling cascade in various human cancers, correlating with increased tumor aggressiveness and drug resistance. [9]. Specifically, high levels of Akt1 expression have been predominantly observed in gastrointestinal stromal tumors, as well as thyroid and breast cancers. Elevated Akt2 expression has been found in hepatocellular carcinoma, glioma, ovarian, colorectal, and pancreatic cancers, whereas Akt3 overexpression has been linked to breast and prostate cancers. In several studies, Akt signaling is also associated with enhanced cell motility and invasion [10].

Akt proteins derive from the cell membrane by PIP3 generated by the phosphorylation of PIP2 by PI3K [11,12]. Due to its relevant role in many important cancer processes, Akt is currently considered a valuable target for the development of new therapeutic agents effective in the treatment and prevention of different types of cancer [13]. In the past years many azole derivatives were described for their significant anticancer properties due to Akt inhibition. In particular triazole and tetrazole nuclei, in both condensed and uncondensed form, were identified as promising scaffolds for the development of novel potent inhibitors of Akt signal [14–17].

Representative examples of Akt inhibitors with triazole structure are reported in Fig. 1. Compounds **1a–c** (Fig. 1) exhibited a significant antiproliferative activity, in the low micromolar range, against colorectal, ovarian and prostate cancer cell lines with a mechanism of action involving the inhibition of the phosphorylation of Akt1 and Akt2 isoforms. In particular, the phosphorylated forms of Akt1 and Akt2 were reduced by 76 % and 86 %, respectively, upon the cell treatment with triazole **1a** at the concentration of 11.5 μM [14]. The triazole derivative **2** (Fig. 1) proved to be active as anticancer agent in the treatment of human glioblastoma (U87MG) and ovarian carcinoma (A2780) by strongly inhibiting TORC1/p70S6K/S6 pathway downstream from Akt [15]. Derivative **3** (Fig. 1) was indeed described for its potent *in vitro* and *in vivo* activity against prostate cancer. Mechanistic studies elucidated that the triazole **3** acts through the inhibition of PI3K/ Akt activity, leading to the hindrance of mTOR signaling pathways and a down-regulation of the oncoprotein c-Myc, which decreases cyclin D1 protein expression and induces G1 arrest of the cell cycle and apoptosis [16].

Analogously, compound MM129 (Fig. 1), bearing a tetrazole nucleus fused with a pyrazolo and a triazine ring, showed strong inhibitory activity, in the low micromolar range, towards two colorectal cancer cell lines, DLD-1 and HT-29, successfully reducing cancer development *in vivo* in colon cancer xenograft mice. These effects have been correlated to a decrease in the expression of Akt, CDK2, mTOR, and programmed death-ligand 1 (PD-L1) [17,18].

In the present paper, considering the established value of Akt as an anticancer target and inspired by the promising results achieved with the triazole and tetrazole compounds in this field, we synthesized new derivatives, bearing these two scaffolds, as Akt inhibitors. The new derivatives present structural features that appear advantageous for the interaction with the ATP binding site of AKT, in particular the nitrogen atoms of the azole scaffold could act as hydrogen bond acceptors with the residues Ala 230, Asp 292, Thr 211. Moreover, the ureidic portion could improve the affinity towards the protein, furnishing the sites for additional hydrogen bonds.

Additionally, the relevant role of pyrrolidine [19] and piperidine nuclei [20] in the development of new Akt inhibitors has been widely reported. Representative examples are the pyrrolidine compounds **4a–d** (Fig. 1) and the piperidine derivative AZD5363 (Fig. 1). Compounds **4a–d** showed potent *in vitro* and *in vivo* antiproliferative activity against prostate (PC3) and colorectal (Colo205) carcinomas due to a strong Akt inhibition, exhibiting IC_{50} values ranging from 0.5 to 7.7 nM. Analogously, AZD5363, also known as capivasertib, was recently approved for

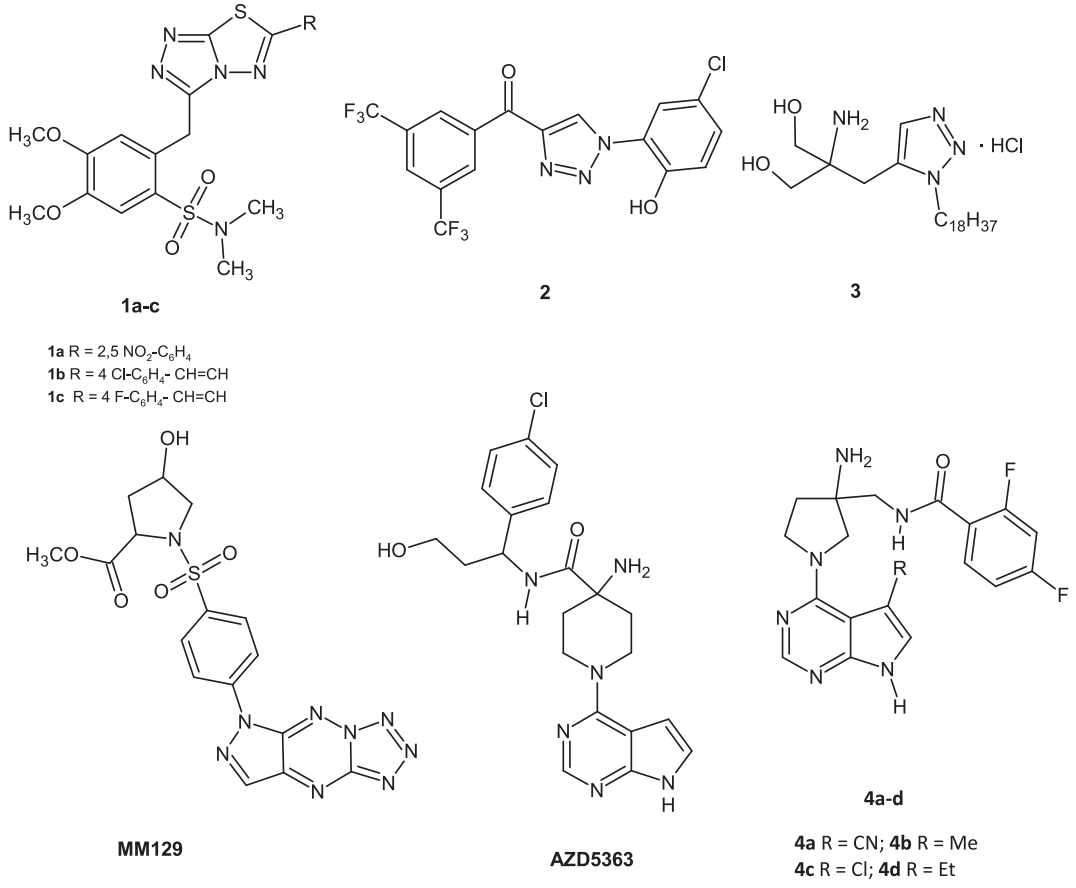

Fig. 1. Chemical structures of known Akt inhibitors with anticancer activity [14–17].

the treatment of breast cancer because of its strong ability to inhibit all the three Akt isoforms with IC_{50} values lower than 10 nM.

Therefore, on the basis of the interesting Akt inhibitory activity described for pyrrolidine and piperidine compounds, we decided to synthesize analogues in which the central azole nucleus was functionalized with these moieties.

Considering the importance of the PI3K-AKTmTOR signaling pathway in the etiology and poor prognosis of pancreatic cancer [21,22] and our interest in the development of new therapeutic approaches for this disease [23–29], we evaluated the new compounds against a panel of pancreatic cancer cell lines.

2. Results and discussion

2.1. Chemistry

Initially we synthesized the 1,2,3-triazole ureas, bearing the pyrrolidine moiety, **9a,b, 10a,b** and **12a,b** following the synthetic procedure reported in Scheme 1. The key intermediates **6a,b** were obtained in good yields (72–74 %) by heating the suitable benzaldehyde **5,** under nitrogen atmosphere, with sodium azide and nitromethane in presence of sodium sulfite and sodium bisulfite [30]. The reaction of compound **6** with 1-pyrrolidinecarbonyl chloride **8** in tetrahydrofuran in presence of triethylamine and 4-dimethylaminopyridine (4-DMAP) allowed to obtain the desired derivatives **9a,b** (yields 60 %, 62 %) mixed with the corresponding N2 isomers **10a,b** (yields 24 %, 22 %). The mixtures were separated by chromatography column to obtain the four isomers as pure compounds. The required carbonyl chloride **8** was obtained by treating the pyrrolidine **7** with triphosgene in presence of sodium bicarbonate in anhydrous dichloromethane at −10 °C.

The reaction of the bromo analogue **9b**, with the suitable phenylboronic acid **11** in dioxane, in presence of potassium carbonate as base and $PdCl_2$(dppf) as catalyst, under nitrogen at 80 °C for two hours, gave compounds **12a,b** in good yields (88 %, 81 %).

Then we decided to synthesize the new analogs **14a,b**, **15b** and **16,** in which the pyrrolidine ring was replaced with a piperidine moiety (Scheme 2).

Derivatives **14** were prepared by the reaction of the suitable intermediate **6** with the carbonyl chloride **13**, under the same reaction conditions (Scheme 2). As observed for the analogues **9**, also in the case of compound **14b** (yield 70 %), it was obtained in mixture with the corresponding N2 isomer **15b** (yield 18 %); no isomer has indeed been isolated in the case of the derivative **14a** (yield 68 %) because of its very low yield. The carbonyl chloride **13** was prepared in situ, by the piperidine treated with triphosgene in anhydrous tetrahydrofuran added with diisopropylethylamine at 0 °C. Finally, compound **16** was obtained by the reaction of the bromo analogues **14b** with 3-hydroxymethyl phenylboronic acid in dioxane, in presence of potassium carbonate as base and $PdCl_2$(dppf) as catalyst.

The synthesis of the new derivatives, **19** and **20a,b**, in which the central triazole scaffold of derivatives **14**–**16** was replaced with the tetrazole isomer (Scheme 3) started by heating at 100 °C the 4-bromobenzonitrile **17** with sodium azide in anhydrous toluene, in presence of trimethylamine, to obtain the tetrazole intermediate **18**. The latter

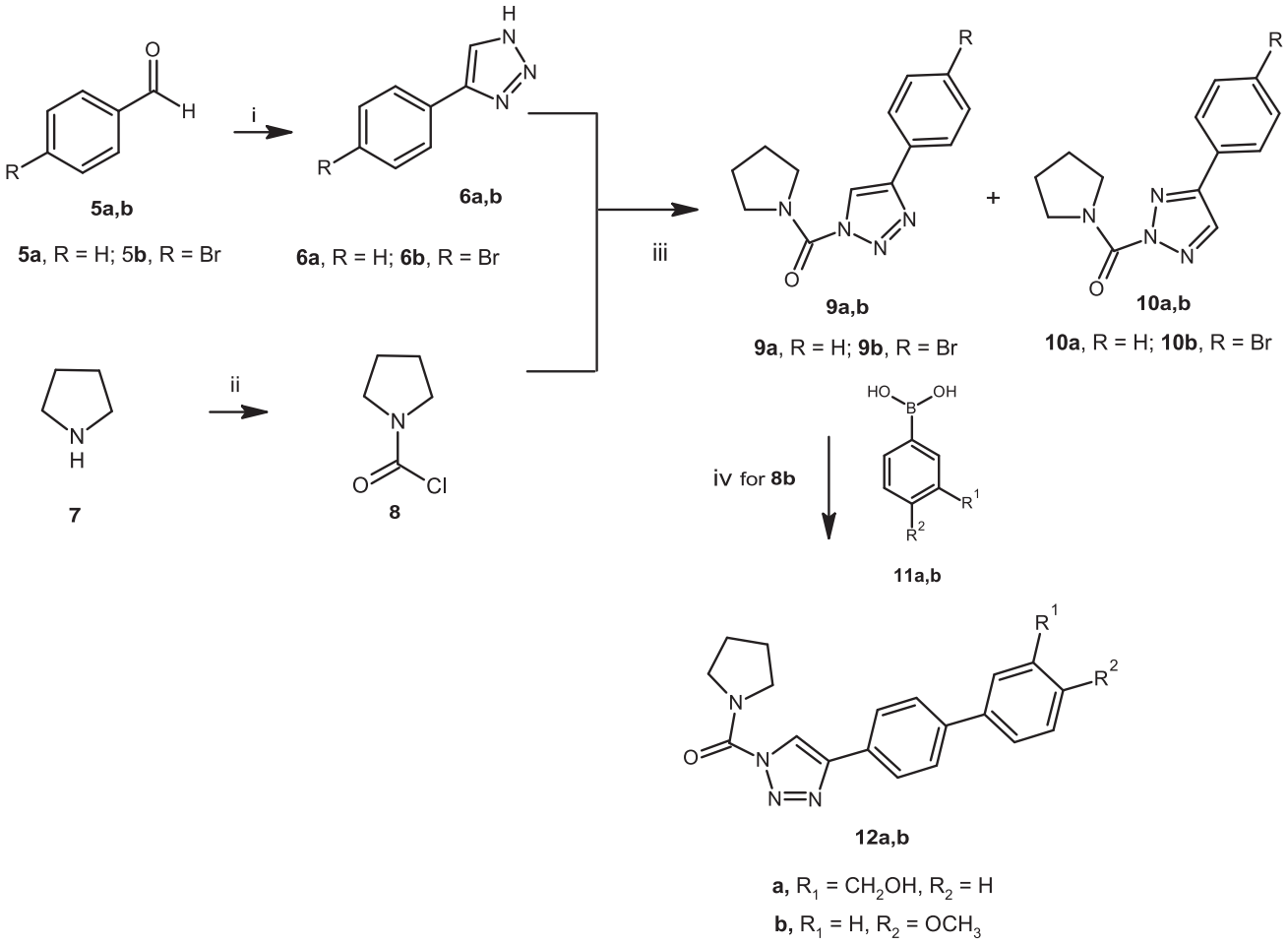

Scheme 1. Synthesis of 1,2,3-triazole ureas **9, 10** and **12.** Reagents and conditions: i) NaN_3, $NaHSO_3$, Na_2SO_3, CH_3NO_2, DMSO 110 °C, under nitrogen, 3 h; ii) triphosgene, anhydrous DCM, $NaHCO_3$, −10 °C, r.t., 6 h; iii) anhydrous THF, DMAP, triethylamine, 60 °C, 10 h; iv) dioxane, water, phenylboronic acid, K_2CO_3, $PdCl_2$(dppf), under nitrogen, 80 °C, 2 h.

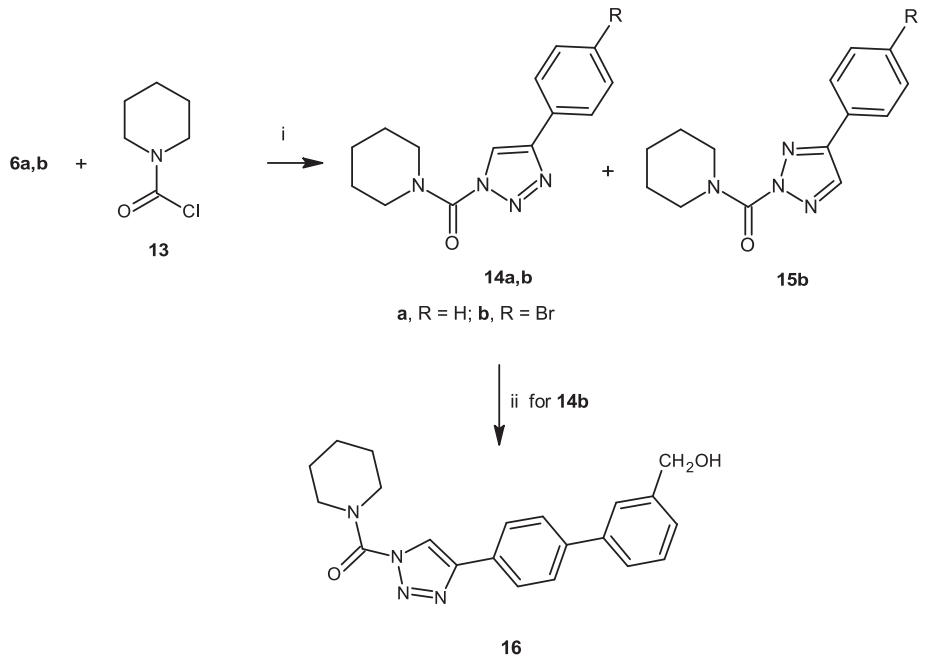

Scheme 2. Synthesis of the piperidine analogues **14a**, **14b**, **15b** and **16**. Reagents and conditions: i) anhydrous THF, diisopropylethylamine, DMAP, 4-phenyltriazole **6a,b**, 60 °C, 2–10 h; ii) dioxane, water, phenylboronic acid, K_2CO_3, $PdCl_2$(dppf), under nitrogen, 80 °C, 2 h.

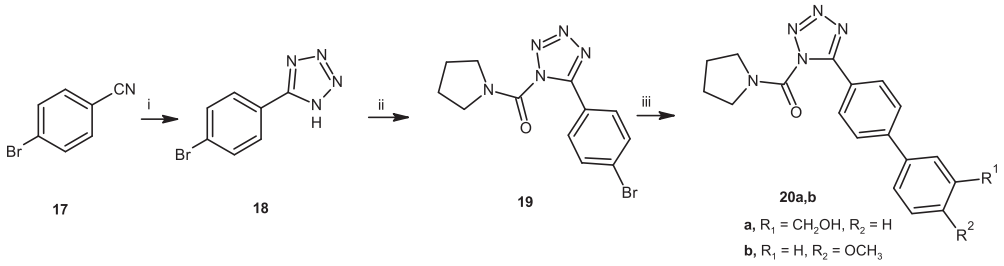

Scheme 3. Synthesis of tetrazole ureas **19** and **20a,b.** Reagents and conditions: i) NaN_3, triethylamine hydrochloride, toluene, 100 °C, 24 h; ii) anhydrous THF, triethylamine, DMAP, pyrrolidine-1-carbonyl chloride **7**, 60 °C, 10 h; iii) dioxane, water, potassium carbonate, $PdCl_2$(dppf), phenylboronic acid **11a,b**, under nitrogen, 80 °C, 2 h.

was reacted with pyrrolidine-1-carbonyl chloride **8** in anhydrous tetrahydrofuran at 60 °C in order to give the urea derivative **19**. In the end, through the reaction of the bromo derivative **19** (yield 80 %); with the suitable phenyboronic acid **11** we achieved the tetrazole analogues **20a, b** (yields 89 %, 85 %).

The ^{1}HNMR spectra of derivatives **9a,b, 10a,b, 12, 19** and **20a,b** showed the characteristic signals of the eight protons (4 × CH_2) of the pyrrolidine scaffold in the range 1.96–4.08 δ, whereas, the spectra of the piperidine analogs, **14a,b**, **15b** and **16** displayed a multiplet for six protons in the range 1.67–1.76 δ, and a broad singlet around 3.80 δ related to the other four protons of the piperidine ring. Importantly, the two couples of triazole isomers **9**–**10** and **13**–**14** were ricognized by the different chemical shift of the triazole hydrogen, which was at 8.49–8.50 for the N1 isomers **9** and **13**, and 8.00–8.07 δ for the N2 isomers **10** and **14.** The ^{13}CNMR spectra of all the new synthesized azole urea compounds showed an upfield shift of the carbonyl carbon peak in the range147.1–162.8 δ due to the effect of vicinal endocyclic nitrogen atoms.

2.2. Biological evaluation

2.2.1. In vitro antiproliferative activities

The newly synthesized compounds **9a,b**, **10a,b**, **12a,b**, **14a,b**, **15b, 16** and **20a,b**, were initially screened at three doses (10, 1, and 0.1 μM) for evaluating their antiproliferative activity against two PDAC immortalized cell lines (PANC-1 and PATU-T) using the Sulforhodamine B (SRB) assay (Fig. 2).

The derivatives **9a, 10a, 14a** and **15b**, which exhibited the highest potency against the two cancer cell lines, showing a percentage of inhibition greater than 50 % when tested at 10 μM, were subsequently tested at lower concentrations in order to determine their IC_{50} values against the PDAC cells PANC-1, PATU-T and SUIT-2 (Table 1). Among selected compounds, triazole **14a**, bearing a piperidine moiety in position N1 and a phenyl ring in position 4, displayed the highest antiproliferative activity against the above-mentioned three PDAC cell lines tested, with IC_{50} values ranging from 1.32 to 3.85 μM. To further assess the anticancer potential of compound **14a** against pancreatic cancer, it was evaluated *in vitro* on the BxPC-3 (K-ras non-mutated cells), yielding IC_{50} of 10.6 μM. In addition, we conducted parallel experiments with clinically used drugs, gemcitabine and 5-fluorouracil (5-FU), as shown in Supplementary Table 1. Gemcitabine demonstrated activity at low nanomolar concentrations, consistent with previous studies [31]. However, the IC_{50} values of 5-FU ranged between 4.4 (SUIT-2) and 7.0 μM (PATU-T), which were comparable to those observed for our new compounds.

2.2.2. In vitro cell cycle analysis

Akt promote cell cycle progression mainly by facilitating the G1 to S

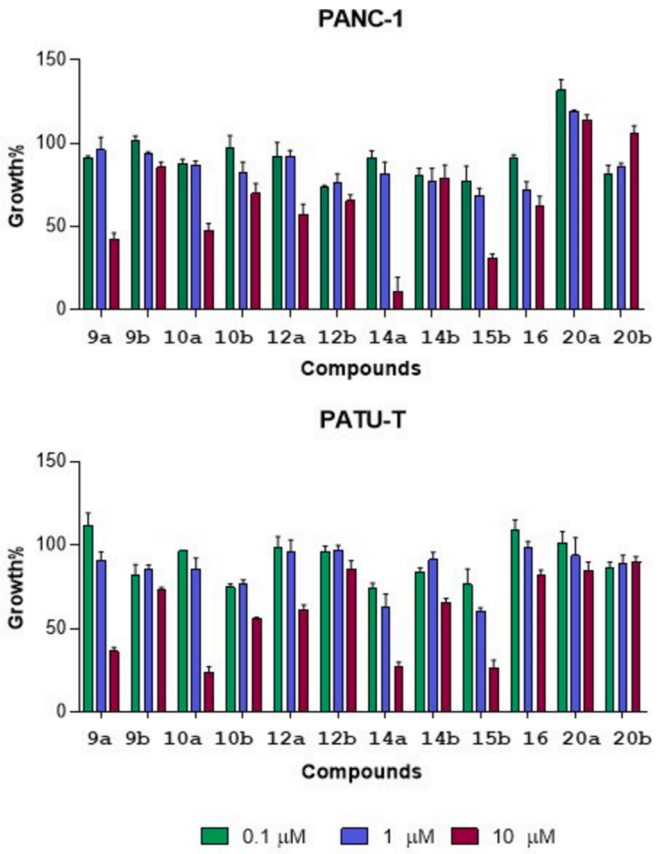

Fig. 2. Antiproliferative activity of the new compounds **9a,b**, **10a,b**, **12a,b**, **14a,b**, **15b, 16** and **20a,b**, evaluated as growth inhibition in PANC-1 and PATU-T cell lines at three screening concentrations (0.1, 1 and 10 μM).

Table 1
Antiproliferative activity of the compounds **9a, 10a, 14a** and **15b** against PDAC cells.

Cpd	IC_{50}[a](μM) ± SEM[b]		SUIT-2
	PANC-1	Patu-T	
9a	5.81 ± 0.14	2.38 ± 0.05	8.29 ± 0.08
10a	5.39 ± 0.1	2.37 ± 0.03	8.89 ± 0.04
14a	3.05 ± 0.07	1.32 ± 0.05	3.85 ± 0.06
15b	6.31 ± 0.03	1.55 ± 0.08	5.32 ± 0.03

[a] The values are means ± SEM of three separate experiments.
[b] SEM: Standard Error of the Mean.

phase transition through inhibition of the cyclin-dependent kinase inhibitors p21 and p27. Therefore, pharmacological inhibition of the Akt prevents G1 cell cycle progression into S, resulting in G1 accumulation [32]. To better understand the antiproliferative mechanism on cancer cells, we performed a cell cycle analysis on PATU-T cells after a 24-h incubation with the compound **14a**. Cell cycle progression was analyzed by cytofluorimetry, using propidium iodide (3,8-diamino-5-[3-(diethylmethylammonio)propyl]-6phenyl-diiodide, PI) staining solution (Fig. 3). In line with our hypothesis regarding the inhibitory effect on Akt, compound **14a** increased the percentage of cells in the G1 phase, rising from 25 % to 50 % and 60 % following exposure to the IC_{50} and 5-fold IC_{50} concentrations, respectively.

2.2.3. *Wound healing assay: Antimigratory evaluation*

Since PDAC is notoriously an aggressive malignancy, with metastasis significantly contributing to the elevated mortality rate, the antimigratory activity of the most active derivative **14a**, was *in vitro* evaluated by the wound healing assay (Fig. 4). A confluent layer of cells was scratched with a specific tool and the ability of the cells to migrate was assessed over a period of 24 h after treatment using a phase-contrast microscopy. Consequently, compound **14a** was tested on the three aforementioned PDAC cell lines at concentrations equal to 5 times the IC_{50} (5× IC_{50}) values. Notably **14a** reduced cell migration against all PDAC cell lines without causing cell death, within the 24 h of this assay. Interestingly, compound **14a** showed a significant reduction of cell migration against PANC-1 already after 8 h from the scratch and subsequent treatment. Remarkably, after 20 and 24 h, in the control groups the cell migration appeared complete and the wound closed whereas in the layers of cells treated with the compound, a significant reduction in migration was observed in all the tested cancer cells, showing a percentage of migration of 31.5, 44.5 and 33 % in PANC-1, PATU-T and SUIT-2, respectively. In summary, **14a** achieved *in vitro* promising cell migration inhibition, indicating its potential targeting cancer cell metastasis.

2.2.4. *Effects on 3D model: Spheroids*

The promising results encouraged us to further investigate the activity of our most promising compound **14a** on a three-dimensional (3D) model of PATU-T. Spheroids better mimic the real 3D architecture of tumours respect the traditional 2D cell cultures, providing more reliable results regarding the evaluation of tumor growth, cell–cell interactions, and drug responses. The 3D model employed in the assay was obtained by plating 3500 cells/well in appropriate 96 U bottom plates. Following a three-day incubation period (Day 1), the spheroids were treated with compound **14a** at a concentration of five times the IC_{50} value on Days 1 and 4. The experiment was then monitored taking pictures for nine days using phase-contrast microscopy. As shown in the Fig. 5, spheroids treated with compound **14a** significantly reduced tumor cells proliferation and spheroids volume after 9 days from the first treatment. This

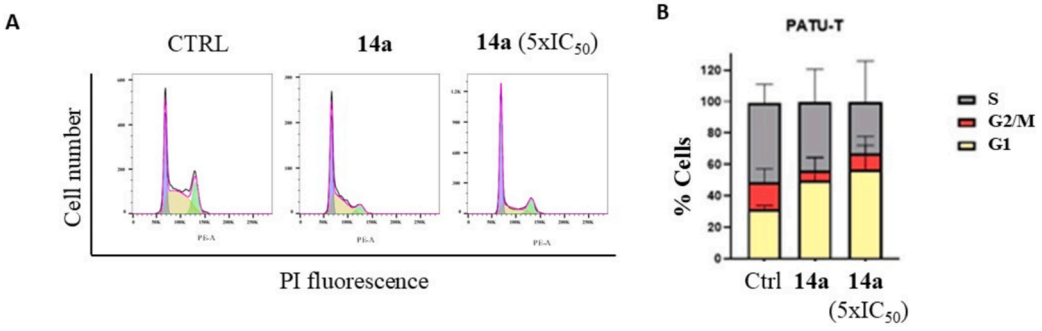

Fig. 3. A Effects of triazole compound **14a** on cell cycle modulation. PATU-T cells were treated for 24 h. **B** Stacked bar graphs show the mean percentage of cells at various stages of cell cycle, G1 (yellow), S (grey), and G2/M (red) phase, in untreated control and after treatment with the compound. Error bars report standard deviations of three separate experiments**.** (For interpretation of the references to colour in this figure legend, the reader is referred to the web version of this article.)

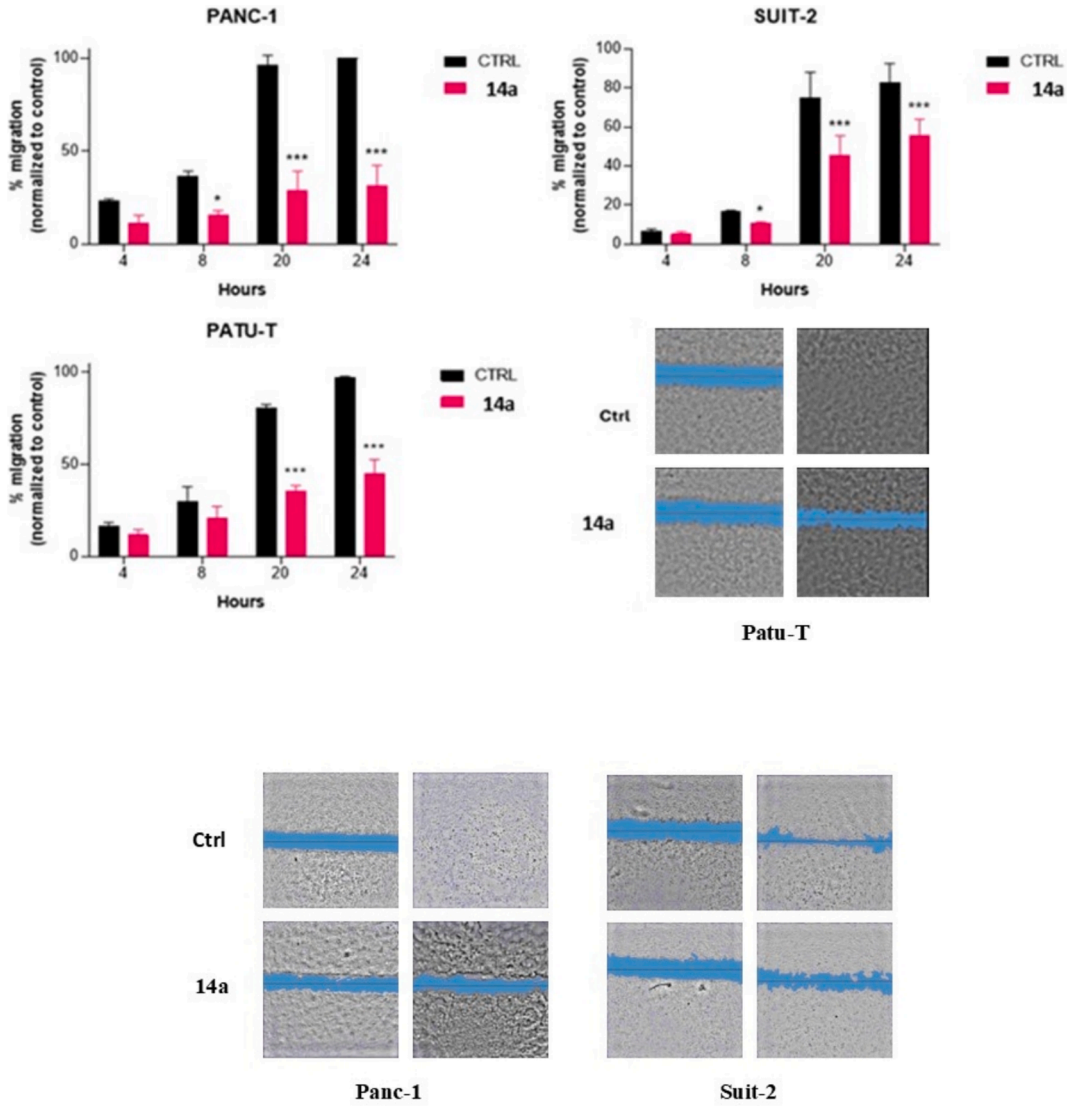

Fig. 4. The cell migration of PATU-T, PANC-1 and SUIT-2 monitored over 24 h. Data are expressed as mean ± SD of two experiments performed in duplicate.***p < 0.001, **p < 0.01, *p < 0.05.

reduction was quantified at over 24 % compared to the control group, which is considered a potentially biologically and clinically relevant result. According to the RECIST criteria used in clinical settings, a reduction in tumor volume of more than 30 % is classified as a response, while a "stable disease" typically reflects a change of less than 20 % in the sum of the diameters of the target lesions. Thus, compound **14a** demonstrated its antiproliferative activity against PATU-T cell in both 2D and 3D models.

2.2.5. Target insights: Phospho-kinases inhibition

To investigate the specific kinase inhibitory activity of compound **14a**, a kinase profiling test was conducted on PATU-T cells using the Proteome Profiler Human Phospho-Kinase Array Kit (R&D, ARY003C). This kit detects the relative levels of phosphorylation of 37 kinase sites and 2 related total proteins. As illustrated in Fig. 6, after a 2-h incubation with a dose of 6.6 μM (5 × IC_{50}), the cells were lysed and the array was performed. Among the screened kinases, compound **14a** more potently inhibited phospho-Akt, showing a 53 % reduction in phosphorylation compared to the untreated control.

2.2.6. Evaluation of apoptosis induction

Akt plays a crucial role in the pathogenesis of cancer by acting as an anti-apoptotic signaling molecule. Its overexpression is often associated with enhanced cell ability to survive even in adverse conditions. The induction of apoptotic response after exposure to compound **14a** at IC_{50} levels was evaluated in both PATU-T and SUIT-2 cells (Fig. 7).

The apoptotic index was evaluated as the percentage of cells exhibiting chromatin condensation and nuclear fragmentation relative to the total cell count.

2.2.7. ELISA assay

The anticancer mechanism of action involving the Akt inhibition was confirmed by evaluating, through an ELISA assay, the modulation effect of compound **14a** on Akt protein activation. Akt phosphorylation at serine 473 (pS473Akt) was analyzed in PATU-T and SUIT-2 cells, treated with the compound at its IC_{50} concentration for 2 h and, as reported in Fig. 8, a significant Akt phosphorylation inhibition was observed in the treated cells respect to the control.

3. Conclusions

A new series of triazole and tetrazole urea derivatives was efficiently synthesized and evaluated for its anticancer properties against pancreatic cancer. The most active compounds, **9a, 10a, 14a** and **15b**, shared a

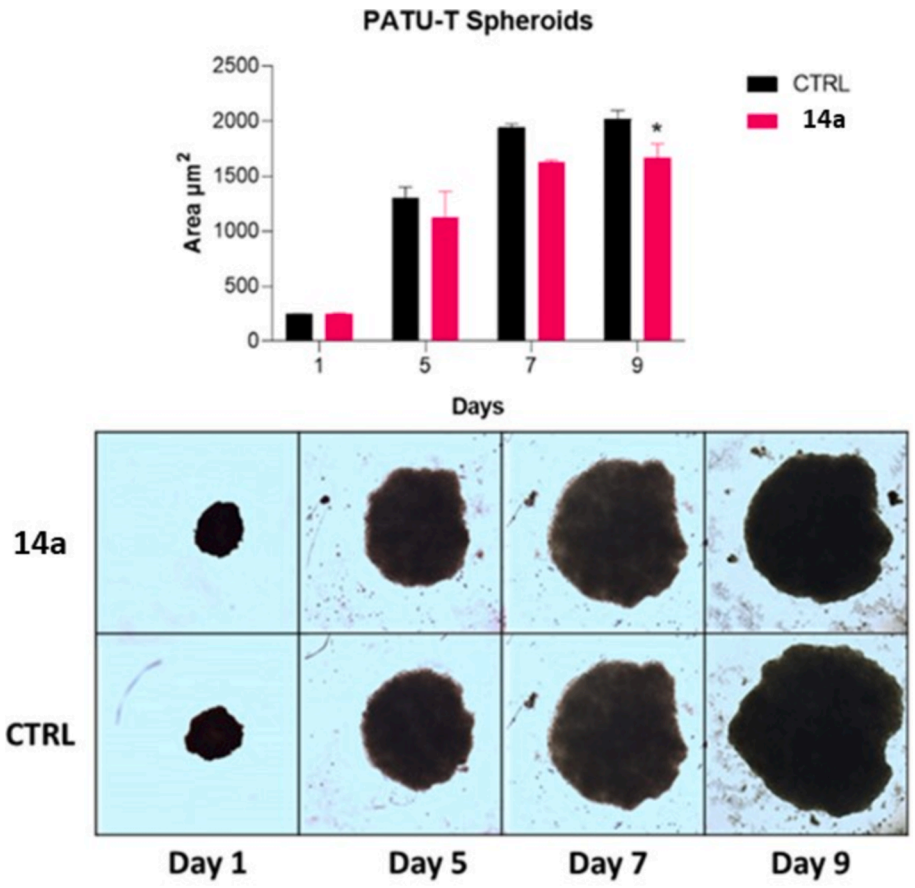

Fig. 5. A) Bar plot shows spheroids area changes in treated and untreated conditions. Data are expressed as mean ± SD of two experiments performed in duplicate. ***p < 0.001, **p < 0.01, *p < 0.05. B) Representative images of PATU-T spheroids.

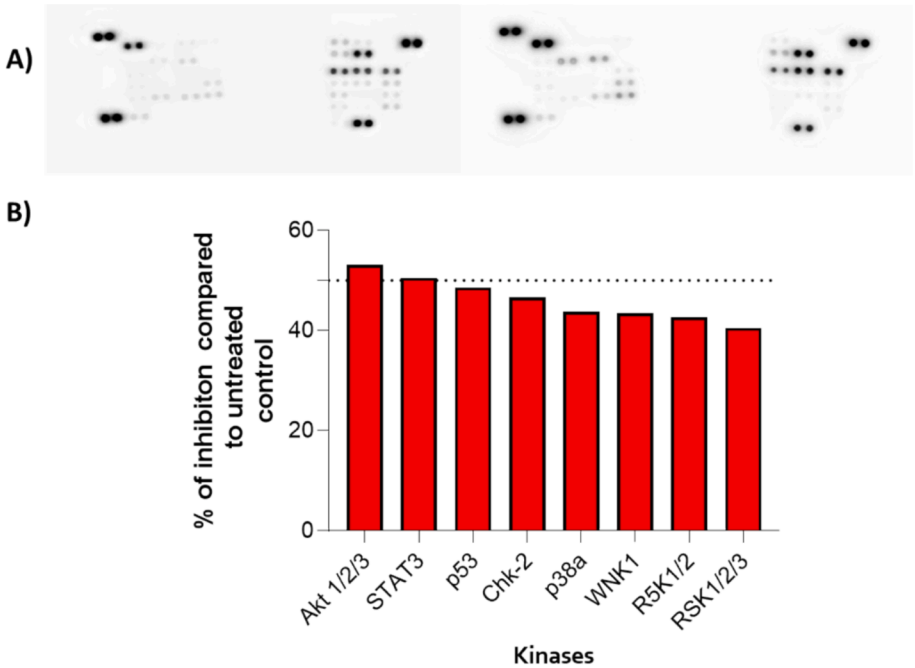

Fig. 6. A) Representative images of pictures after the development of the control array (left) and the treated array (right). B) bar plot illustrates the inhibition of kinases phosphorylation after treatment with **14a**.

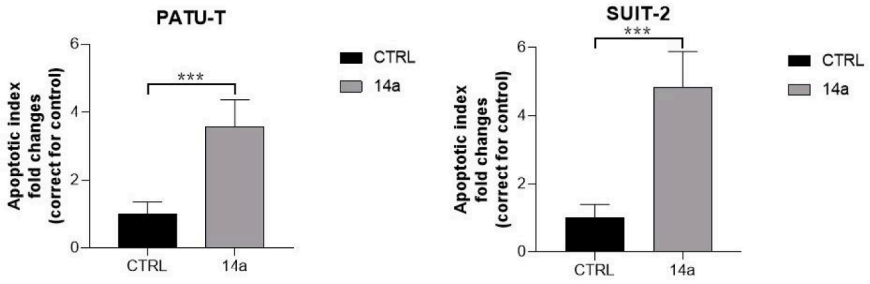

Fig. 7. Apoptotic index of compound **14a** evaluated in PATU-T and SUIT-2 cells. Measurements were performed in triplicate. P values were calculated with Student's *t*-test. ****p < 0.0001, ***p < 0.001, **p < 0.01, *p < 0.05, ns = not significant.

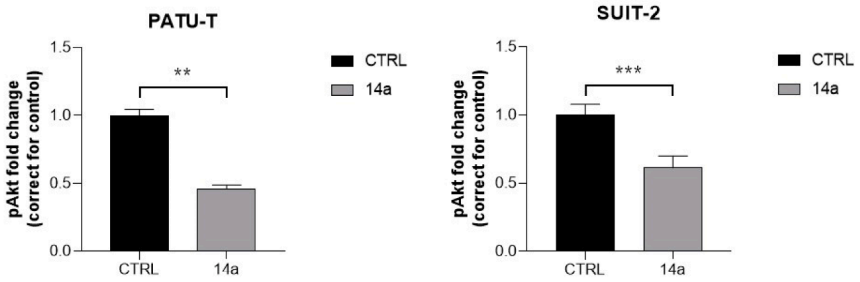

Fig. 8. Effect of compound **14a** on Akt phosphorylation at serine 473 (pS473Akt). The levels of pS473Akt were quantified in PATU-T and SUIT-2 cells. Measurements were performed in triplicate. P values were calculated with Student's *t*-test. ****p < 0.0001, ***p < 0.001, **p < 0.01, *p < 0.05, ns = not significant.

common structural feature: a central triazole ring substituted with a carbonyl pyrrolidine or piperidine at the N1 or N2 position, and bearing a phenyl ring, unsubstituted or brominated, at the 4-position. Noteworthy, triazole central core proved to be crucial for the activity, in fact its replacement with the tetrazole ring appears detrimental for the anticancer activity. Triazole **14a**, bearing a piperidine moiety in position N1 and a phenyl ring in position 4, exhibited the highest antiproliferative activity against the three PDAC cell lines tested, PANC-1, PATU-T and Suit-2, eliciting IC_{50} values ranging from 1.32 to 3.85 μM. Interestingly, this antiproliferative activity has also been confirmed in a 3D spheroid model of PATU-T cells. Considering the significant role played by metastases in the aggressiveness of pancreatic cancer, the anti-migratory activity of compound **14a** was evaluated in a wound healing assay and a significant inhibition of cell migration in PANC-1 was observed already after 8 h from the scratch. To further investigate the mechanism of action of compound **14a** as a kinase inhibitor, a Proteome Profiler Human Phospho-Kinase assay was performed to investigate the inhibitory activity of kinases phosphorylation in PATU-T cells. These results highlighted a potent inhibition of Akt phosphorylation, which was validated by specific ELISA assays. This inhibition determines an alteration of the downstream PI3K/AKT/mTOR signaling pathway, which plays a crucial role in cell survival, proliferation and migration, resulting in anti-proliferative and anti-migratory effects in tumors [33,34]. However, we also observed an inhibition of the STAT3 pathway. Of note, Akt and STAT3 pathways are interconnected through various mechanisms, and their interplay is crucial for regulating cellular functions. In particular, activated Akt can phosphorylate and enhance the activity of various components in the STAT3 pathway, including JAKs. This cross-talk can potentiate the signaling effects of both pathways, leading to enhanced cell survival and proliferation [35]. This mechanism was further studied by the analysis of apoptosis, which showed a significant induction of apoptosis after treatment with the derivative **14a**.

An important limitation of the current study is that we did not perfom in vivo studies. However, although in vivo models offer critical insights into pharmacokinetics, toxicity, and therapeutic efficacy, they generally represent a subsequent phase in drug development following the establishment of robust *in vitro* results, as presented here. These studies allow for a preliminary understanding of molecular mechanisms, informing which compounds warrant further investigation. Thus, we intend to pursue in vivo studies as a natural progression of our research to confirm and expand upon the promising findings of this initial work in future studies

Altogether, the obtained results revealed the promising anticancer properties of derivative **14a**, which can be considered a valuable lead compound for the development of new therapeutic approaches in the treatment of PDAC.

4. Experimental section

All materials and solvents were purchased from Merck, VWR International, Alfa Aesar and Acros Organics, and used without further purification. A Buchi-Tottoly capillary instrument was employed for the melting points evaluation (Büchi, Cornaredo, Italy) and have not been corrected. ^{1}H and ^{13}C spectra were acquired at 200 and 50 MHz, respectively in $CDCl_3$ solution, using a Bruker Avance II series 200 MHz spectrometer (Bruker, Milan, Italy). Column chromatography was performed with Merck silica gel 230–400 mesh ASTM or with a Büchi Sepacor chromatography module (prepacked cartridge system). Elemental analyses (C, H, N) were within ±0.4 % of theoretical values and were performed with a VARIO EL III elemental analyzer.

4.1. Chemistry

4.1.1. General synthesis of 4-phenyl-1H-1,2,3-triazole *6a,b*

A mixture of benzaldheyde **5** (3.9 mmol), sodium azide (17 mmol),

sodium bisulfite (4 mmol), sodium sulfite (4 mmol) and DMSO (8 ml) was heated at 110 °C, under nitrogen atmosphere. Then, a solution of nitromethane (8 mmol) in DMSO (4 ml) was added dropwise over 2 h. The reaction mixture was heated under reflux for further 3 h and then cooled to room temperature, poured into 80 ml of water and extracted with ethyl acetate (3 × 30 ml). The organic layers were washed with water and brine and then dried over anhydrous Na_2SO_4, filtered and evaporated *in vacuum*. The crude product obtained was purified by silica gel column chromatography using dichloromethane: ethyl acetate, 1:1 as eluent (yields: 72–74 %). Spectroscopic data were in accordance to those previously reported [30].

4.1.2. Synthesis of pyrrolidine-1-carbonyl chloride *7*

A solution of pyrrolidine (10 mmol) in anhydrous dichloromethane (1.66 ml) was slowly added at −10 °C to a mixture of sodium bicarbonate (20 mmol) and triphosgene (6.5 mmol) in anhydrous dichloromethane. The resulting reaction mixture was then stirred at room temperature for 6 h, then it was filtered and evaporated *under vacuum*. The obtained product was directly used for the subsequent synthetic steps without further purification [36].

4.1.3. General synthesis of (4-phenyl-1,2,3-triazolyl)(pyrrolidin-1-yl) methanones ***9a,b*** and ***10a,b***

A mixture of pyrrolidine-1-carbonyl chloride **7** (10 mmol), suitable 4-phenyl-1*H*-1,2,3-triazole **5** (12 mmol), DMAP (1.23 g), in anhydrous tetrahydrofuran (16.6 ml) and triethylamine (3.4 ml), was heated at 60 °C for 10 h. The solvent was removed at reduced pressure to obtain the crude product, which was purified by silica gel column chromatography eluting by dichloromethane to give the pure compounds **9a,b** and their diasteroisomers **10a,b**.

*4.1.3.1. (4-Phenyl-1H-1,2,3-triazol-1-yl)(pyrrolidin-1-yl)methanone **9a**.* Yield: 60 %, m.p.: 200.7 °C. R.f. (ethyl acetate:cyclohexane, 1:1) 0.69. ^{1}HNMR (200 MHz, $CDCl_3$) δ: 1.97–2.07 (4H, m, 2× CH_2), 3.76 (2H, t, J = 6.5 Hz CH_2), 4.08 (2H, t, J = 6.5 Hz, CH_2), 7.37–7.50 (3H, m, Ar—H), 7.81–8.01 (2H, m, Ar—H), 8.50 (1H, s, CH-triazole). ^{13}C NMR (50 MHz, $CDCl_3$) δ: 23.9 (t), 26.6 (t), 49.0 (t), 50.3 (t), 120.2 (d), 125.9 (d × 2), 128.6 (d), 128.9 (d × 2), 129.6 (s), 146.4 (s), 147.1 (s). Anal. Calcd for $C_{13}H_{14}N_4O$ (MW: 242.77): C, 64.45; H, 5.82; N, 23.13 %. Found: C, 64.68; H, 5.97; N, 23.41 %.

*4.1.3.2. [4-(4-Bromophenyl)-1H-1,2,3-triazol-1-yl](pyrrolidin-1-yl)methanone **9b**.* Yield: 62 %, m.p.: 183–184 °C. R.f. (ethyl acetate:cyclohexane, 1:1) 0.70. ^{1}HNMR (200 MHz, $CDCl_3$) δ: 1.97–2.07 (4H, m, 2× CH_2), 3.75 (2H, t, J = 6.5 Hz, CH_2), 4.07 (2H, t, J = 6.5 Hz, CH_2), 7.58 (2H, d, J = 8.5 Hz, Ar—H), 7.76 (2H, d, J = 8.5 Hz, Ar—H), 8.49 (1H, s, CH-triazole). ^{13}C NMR (50 MHz, $CDCl_3$) δ: 23.9 (t), 26.5 (t), 49.0 (t), 50.3 (t), 118.2 (s), 120.4 (d), 125.2 (d × 2), 126.4 (s), 129.9 (d × 2), 143.2 (s), 144.7 (s). Anal. Calcd for $C_{13}H_{13}BrN_4O$ (MW: 321.17): C, 48.62; H, 4.08; N, 17.44 %. Found: C, 48.83; H, 4.31; N, 17.62 %.

*4.1.3.3. (4-Phenyl-2H-1,2,3-triazol-2-yl)(pyrrolidin-1-yl)methanone **10a**.* Yield: 24 %, m.p.: 173.5 °C. R.f. (ethyl acetate:cyclohexane, 1:1) 0.58. ^{1}HNMR (200 MHz, $CDCl_3$) δ: 1.96–2.03 (4H, m, 2× CH_2), 3.77 (2H, t, J = 6.6 Hz CH_2), 3.94 (2H, t, J = 6.6 Hz, CH_2), 7.44–7.47 (3H, m, Ar—H), 7.86–7.90 (2H, m, Ar—H), 8.07 (1H, s, CH-triazole). ^{13}C NMR (50 MHz, $CDCl_3$) δ: 24.1 (t), 26.5 (t), 48.7 (t), 50.2 (t), 99.9 (s), 126.4 (d), 128.9 (d × 2), 129.1 (d), 129.4 (d), 133.1 (d), 147.9 (s), 149.0 (s). Anal. Calcd for $C_{13}H_{14}N_4O$ (MW: 242.27): C, 64.45; H, 5.82; N, 23.13 %. Found: C, 64.61; H, 5.99; N, 23.36 %.

*4.1.3.4. [4-(4-Bromophenyl)-2H-1,2,3-triazol-2-yl](pyrrolidin-1-yl)methanone **10b**.* Yield: 22 %, m.p.: 164.3 °C. R.f. (ethyl acetate:cyclohexane, 1:1) 0.59. ^{1}HNMR (200 MHz, $CDCl_3$) δ: 1.97–2.04 (4H, m, 2× CH_2), 3.73–3.80 (2H, m, CH_2), 3.91 (2H, t, J = 6.3 Hz, CH_2), 7.59 (2H, d, J = 8.5 Hz, Ar—H), 7.75–7.79 (2H, m, Ar—H), 8.04 (1H, s, CH-triazole). ^{13}C NMR (50 MHz, $CDCl_3$) δ: 22.1 (t), 24.4 (t), 46.7 (t), 48.1 (t), 121.5 (s), 125.9 (d × 2), 126.0 (s), 130.1 (d × 2), 130.9 (d), 145.7 (s), 145.9 (s). Anal. Calcd for $C_{13}H_{13}BrN_4O$ (MW: 321.17): C, 48.62; H, 4.08; N, 17.44 %. Found: C, 48.91; H, 4.29; N, 17.67 %.

4.1.4. General synthesis of 4-biphenyl-triazole ureas ***12a,b***

The bromo derivative **8a** (1.15 mmol) was solubilized in a mixture of dioxane (26.4 ml) and water (2.6 ml). The opportune phenyl boronic acid (2.23 mmol), potassium carbonate (4.4 mmol) and the catalyst $PdCl_2$(dppf) were added and the resulting mixture was heated at 80 °C, under nitrogen for 2 h. Once cooled at room temperature, water (50 ml) was added and the mixture was extracted with with ethyl acetate (3 × 30 ml). The organic layers were washed with water and brine, dried over anhydrous Na_2SO_4, filtered and the solvent was removed at reduced pressure. The crude material obtained was purified by silica gel column chromatography using cyclohexane:ethyl acetate, 1:1 as eluent and a subsequent wash with diethyl ether.

*4.1.4.1. {4-[3′-(Hydroxymethyl)biphenyl-4-yl]-1H-1,2,3-triazol-1-yl}(pyrrolidin-1-yl)methanone **12a**.* Yield: 88 %, m.p.: 157.1 °C. ^{1}HNMR (200 MHz, $CDCl_3$) δ: 1.98–2.0.3 (4H, m, 2× CH_2), 2.34 (1H, s, OH), 3.76 (2H, d, J = 6.7 Hz, CH_2), 4.08 (2H, t, J = 6.7 Hz, CH_2), 4.78 (2H, s, CH_2), 7.38–7.57 (4H, m, Ar—H), 7.67 (2H, d, J = 8.3 Hz, Ar—H), 7.92 (2H, d, J = 8.3 Hz, Ar—H), 8.49 (1H, s, CH-triazole). ^{13}C NMR (50 MHz, $CDCl_3$) δ: 23.9 (t), 26.6 (t), 49.1 (t), 50.4 (t), 65.2 (t), 120.2 (d), 125.6 (d), 126.1 (d), 126.2 (d), 126.3 (dx2), 127.6 (dx2), 128.6 (s), 129.1 (d),140.7 (s), 141.1 (s), 141.6 (s), 146.1 (s), 147.1 (s). Anal. Calcd for $C_{20}H_{20}N_4O_2$ (MW: 348.40): C, 68.95; H, 5.79; N, 16.08 %. Found: C, 69.23; H, 5.95; N, 16.31 %.

*4.1.4.2. [4-(4′-Methoxybiphenyl-4-yl)-1H-1,2,3-triazol-1-yl](pyrrolidin-1-yl)methanone **12b**.* Yield: 81 %, m.p.: 217–218 °C. ^{1}HNMR (200 MHz, $CDCl_3$) δ: 2.00–2.03 (4H, m, 2× CH_2), 3.75 (2H, t, J = 6.2 Hz, CH_2), 3.86 (3H, s, OCH_3), 4.08 (2H, t, J = 6.2 Hz, CH_2), 7.00 (2H, d, J = 8.6 Hz, Ar—H), 7.56–7.67 (4H, m, Ar—H), 7.93 (2H, d, J = 8.2 Hz, Ar—H), 8.51 (1H, s, CH-triazole). ^{13}C NMR (50 MHz, $CDCl_3$) δ: 23.9 (t), 26.6 (t), 49.0 (t), 50.4 (t), 55.4(q), 114.3 (d × 2), 120.1 (d), 126.3 (d × 2), 127.1 (d × 2), 127.9 (s), 128.1 (d × 2), 132.9 (s), 141.0 (s), 146.2 (s), 147.1 (s), 159.3 (s). Anal. Calcd for $C_{20}H_{20}N_4O_2$ (MW: 348.40): C, 68.95; H, 5.79; N, 16.08 %. Found: C, 69.21; H, 5.91; N, 16.28 %.

4.1.5. Synthesis of pyperidine-1-carbonyl chloride ***13***

A solution of triphosgene (4.7 mmol) in anhydrous tetrahydrofuran (9 ml) was slowly added to a cooled (0 °C) mixture of piperidine (9.1 mmol), anhydrous tetrahydrofuran (20 ml) and diisopropylethylamine (5.06 ml). At the end of the addition the reaction mixture was left under stirring at 0 °C for additional 30 min. Water (20 ml) was added and the mixture was extracted with ethyl acetate (3 × 20 ml). The organic layers were washed with water and brine, dried over anhydrous Na_2SO_4, filtered and evaporated at reduced pressure. The obtained yellow oil was directly used for the subsequent synthetic steps without further purification [37].

4.1.6. Synthesis of (4-Phenyl-1H-1,2,3-triazol)(piperidin-1-yl)methanones ***14*** and ***15***

4-Dimethylaminopyridine, DMAP, (0.32 g) and triazole 5 (2.4 mmol) were added to a solution of carbonyl chlorides **8** and **13** (10 mmol) in anhydrous tetrahydrofuran (10 ml) and diisopropylethylamine (1.4 ml). The resulting mixture was heated under stirring at 60 °C for 2 h, for the preparation of compound **14a,** and for 10 h, for derivatives **14b** and **15b**. The reaction between 4-(4-bromo phenyl)-1,2,3-triazole **6b** and the piperidine chloride **13** led to the formation of a mixture of both diastereoisomers **14b** and **15b**. After cooling the reaction mixture was poured into a saturated solution of ammonium chloride and extracted

with ethyl acetate (3 × 30 ml). The organic layers were washed with water and brine, dried over anhydrous Na_2SO_4, filtered and evaporated *in vacuo*. The solid was then purified by chromatography column using a mixture cyclohexane:ethyl acetate 1:1 as eluent and a subsequent wash with cool ethyl acetate.

*4.1.6.1. (4-Phenyl-1H-1,2,3-triazol-1-yl)(piperidin-1-yl)methanone **14a**.* Yield: 68 %, m.p.: 129–130 °C ^{1}HNMR (200 MHz, $CDCl_3$) δ: 1.67–1.76 (6H, m, 3× CH_2), 3.81 (4H, bs, 2× CH_2), 7.27–7.50 (3H, m, Ar—H), 7.86–7.90 (2H, m, Ar—H), 8.33 (1H, s, CH-triazole). ^{13}C NMR (50 MHz, $CDCl_3$) δ: 22.7 (t), 24.2 (t), 29.4 (t), 29.7 (t), 31.9 (t), 120.8 (d), 125.9 (d × 2), 128.7 (d), 128.9 (d × 2), 129.6 (s), 146.7 (s), 148.2 (s). Anal. Calcd for $C_{14}H_{16}N_4O$ (MW: 256.30): C, 65.61; H, 6.29; N, 21.86 %. Found: C, 65.93; H, 6.42; N, 21.98 %.

*4.1.6.2. [4-(4-Bromophenyl)-1H-1,2,3-triazol-1-yl](piperidin-1-yl)methanone **14b**.* Yield: 70 %, m.p.: 164.5 °C ^{1}HNMR (200 MHz, $CDCl_3$) δ: 1.70–1.76 (6H, m, 3× CH_2), 3.81 (4H, bs, 2× CH_2), 7.61 (2H, d, J = 8.6 Hz, Ar—H), 7.75–7.91 (2H, m, Ar—H), 8.33 (1H, s, CH-triazole). ^{13}C NMR (50 MHz, $CDCl_3$) δ: 24.2 (t), 25.7 (tx4), 120.9 (d), 122.6 (s), 127.4 (d × 2), 128.6 (s), 132.1 (d × 2), 145.7 (s), 148.0 (s). Anal. Calcd for $C_{14}H_{15}BrN_4O$ (MW: 335.20): C, 50.16; H, 4.51; N, 16.71 %. Found: C, 50.29; H, 4.80; N, 16.93 %.

*4.1.6.3. [4-(4-Bromophenyl)-2H-1,2,3-triazol-2-yl](piperidin-1-yl)methanone **15b**.* Yield: 15 %, m.p.: 129–130 °C ^{1}HNMR (200 MHz, $CDCl_3$) δ: 1.70–1.74 (6H, m, CH_2), 3.70 (4H, bs, CH_2), 7.58 (2H, d, J = 8.6 Hz, Ar—H), 7.75 (2H, d, J = 8.6 Hz, Ar—H), 8.04 (1H, s, CH-triazole). ^{13}C NMR (50 MHz, $CDCl_3$) δ: 24.2 (t × 4), 25.9 (t), 123.5 (s), 127.9 (d × 2), 128.09 (s), 132.2 (d × 2), 132.9 (d), 148.0 (s), 149.2 (s). Anal. Calcd for $C_{14}H_{15}BrN_4O$ (MW: 335.20): C, 50.16; H, 4.51; N, 16.71 %. Found: C, 50.31; H, 4.78; N, 16.98 %.

*4.1.7. General synthesis of 4-biphenyl-triazole ureas **16***

Same procedure described for the synthesis. of the 4-biphenyl-triazole ureas **12a,b,** starting form the brome derivative **14b**.

*4.1.7.1. {4-[3′-(Hydroxymethyl)biphenyl-4-yl]-1H-1,2,3-triazol-1-yl}(piperidin-1-yl)methanone **16**.* Yield: 72 %, m.p.: 102–103 °C ^{1}HNMR (200 MHz, $CDCl_3$) δ: 1.75 (6H, bs, 3× CH_2), 2.13 (2H, s, OH), 3.80 (4H, bs, 2× CH_2), 4.78 (2H, s, CH_2), 7.31–7.61 (3H, m, Ar—H), 7.65–7.70 (3H, m, Ar—H), 7.93 (2H, d, J = 8.0 Hz, Ar—H), 8.34 (1H, s, CH-triazole). ^{13}C NMR (50 MHz, $CDCl_3$) δ: 24.2 (tx4), 25.7 (t), 65.3 (t), 120.9 (d), 125.6 (d × 2), 126.1 (d × 2), 126.3 (d × 2), 127.6 (d × 2), 128.5 (s), 129.1 (d), 140.8 (s), 141.3 (s), 146.4 (s), 147.2 (s), 159.2 (s). Anal. Calcd for $C_{21}H_{22}N_4O_2$ (MW: 362.42): C, 69.59; H, 6.12; N, 15.46 %. Found: C, 69.78; H, 6.34; N, 15.64 %.

*4.1.8. Synthesis of 5-(4-bromophenyl)-1H-tetrazole **18***

A mixture of 4-bromobenzonitrile **13** (9 mmol), sodium azide (9 mmol), triethylamine hydrochloride (9 mmol), and anhydrous toluene (80 ml) was heated at 100 °C for 24 h. After cooling the solution was extracted with water and the aqueous solution was treated dropwise with HCl 37 % until complete precipitation. The white solid obtained was filtered off and washed with water (yield 98 %). Spectroscopic data were in accordance to those previously reported [38].

*4.1.9. Synthesis of [5-(4-bromophenyl)-1H-tetrazol-1-yl](pyrrolidin-1-yl)methanone **19***

A solution of carbonyl chloride **8** (10 mmol), triazole intermediate **14** (8 mmol), anhydrous tetrahydrofuran (17 ml), triethylamine (3.4 ml) and DMAP, (1.23 g) was heated under stirring at 60 °C for 10 h. The solvent was evaporated *under vacuum* and the solid obtained was purified by chromatography column using a mixture dichloromethane:ethyl acetate, 8:2, as eluent.

Yield: 80 %, m.p.: 148.2 °C. ^{1}HNMR (200 MHz, $CDCl_3$) δ: 2.01–2.08 (4H, m, 2× CH_2), 3.58–3.62 (4H, m, 2× CH_2), 7.55–7.61 (2H, m, Ar—H), 7.73–7.86 (2H, m, Ar—H). ^{13}C NMR (50 MHz, $CDCl_3$) δ: 25.6 (t × 2), 47.8 (t × 2), 123;1 (s), 127.0 (d × 2), 132.0 (d × 2), 135.5 (s × 2), 162.0 (s) Anal. Calcd for $C_{12}H_{12}BrN_5O$ (MW: 322.16): C, 44.74; H, 3.75; N, 21.74 %. Found: C, 44.98; H, 3.99; N, 21.88 %.

*4.1.9.1. General synthesis of 4-biphenyl-tetrazole ureas **20a,b**.* Same procedure described for the synthesis. of the 4-biphenyl-triazole ureas **12a,b,** starting from the brome derivative **19b**.

*4.1.9.2. {5-[3′-(Hydroxymethyl)biphenyl-4-yl]-1H-tetrazol-1-yl}(pyrrolidin-1-yl)methanone **20a**.* Yield: 89 %, m.p.: 174.8 °C. ^{1}HNMR (200 MHz, DMSO) δ: 1.93–1.99 (4H, m, 2× CH_2), 3.50 (4H, t, J = 6.7 Hz, 2× CH_2), 4.58 (2H, d, J = 5.7 Hz, CH_2), 5.27 (1H, t, J = 5.7 Hz, OH), 7.36 (1H, d, J = 7.6 Hz, Ar—H), 7.44 (1H, t, J = 7.6 Hz, Ar—H),7.59 (1H, d, J = 7.8 Hz, Ar—H), 7.67 (1H, s, Ar—H), 7.78–7.86 (2H, m, Ar—H), 7.87–7.96 (2H, m, Ar—H). ^{13}C NMR (50 MHz, $CDCl_3$) δ: 22.6 (t × 2), 47.9 (t × 2), 63.3 (t), 123.6 (s), 125.1 (d), 125.5 (d), 126.2 (d × 2), 126.7 (d), 127.8 (dx2), 129.3 (d), 139.3 (s), 142.4 (s), 143.9 (s), 158.2 (s), 162.8 (s). Anal. Calcd for $C_{19}H_{19}N_5O_2$ (MW: 349.38): C, 65.32; H, 5.48; N, 20.04 %. Found: C, 65.58; H, 5.60; N, 20.29 %.

*4.1.9.3. [5-(4′-Methoxybiphenyl-4-yl)-1H-tetrazol-1-yl](pyrrolidin-1-yl)methanone **20b**.* Yield: 85 %, m.p.: 163.7 °C. ^{1}HNMR (200 MHz, DMSO) δ: 1.94–1.97 (4H, m, 2× CH_2), 3.48–3.51 (4H, m, 2× CH_2), 3.80 (3H, s, OCH_3), 7.04 (2H, d, J = 8.3 Hz, Ar—H), 7.67 (2H, d, J = 8.8 Hz, Ar—H), 7.77 (2H, d, J = 8.5 Hz, Ar—H), 7.87 (2H, d, J = 8.4 Hz, Ar—H). ^{13}C NMR (50 MHz, $CDCl_3$) δ: 25.6 (t × 2), 47.9 (t × 2), 55.7 (q), 114.9 (d × 2), 122.9 (s), 126.1 (s), 127.1 (d × 2), 128.3 (d × 2), 131.7 (d × 2), 141.9 (s), 158.2 (s), 159.8 (s), 162.7 (s). Anal. Calcd for $C_{19}H_{19}N_5O_2$ (MW: 349.38): C, 65.32; H, 5.48; N, 20.04 %. Found: C, 65.57; H, 5.71; N, 20.30 %.

4.2. Biology

4.2.1. Drugs and chemicals

The synthesized triazole and tetrazole compounds were dissolved in DMSO. The medium, foetal bovine serum (FBS), penicillin (50 IU mL^{-1}) and streptomycin (50 mg mL^{-1}) were from Gibco (Gaithersburg, MD, USA). All other chemicals were from Sigma (Zwijndrecht, the Netherlands).

4.2.2. Cell culture

The cells were cultured in RPMI-1640 (Roswell Park Memorial Institute 1640) supplemented with 10 % heat-inactivated FBS, 1 % penicillin/streptomycin, or in DMEM (Dulbecco's Modified Eagle's Medium), supplemented with 10 % heat-inactivated FBS, 1 % HEPES. The cells were kept in a humidified atmosphere of 5 % CO_2 and 95 % air at 37 °C and harvested with trypsin-EDTA.

4.2.3. Cell growth inhibition

The cytotoxic activity of the new azole compounds derivatives **9a,b**, **10a,b**, **12a,b**, **14a,b**, **15b**, **16** and **20a,b**, against differentiated pancreatic cancer cells was assessed using the sulforhodamine B (SRB) chemosensitivity assay. Triplicate wells of 96-well flat-bottom plates were seeded with cells in volumes of 100 μL, with 3 × 10^3 cells/well for each cell line SUIT-2, PANC-1 and PATU-T. After incubating for 24 h at 37 °C to allow cells adhesion, the cells were treated with various concentrations of the compounds dissolved in DMSO (100 to allow cells attachment μL) for 72 h at 37 °C, 5 % CO_2, and 95 % humidity.

At the end of incubation period, the cells were fixed with 25 μL of 50 % cold trichloroacetic acid and kept for at least 60 min at 4 °C. Then, the plates were emptied and washed gently with deionized water, dried at room temperature (RT) overnight. and stained with 50 μL of 0.4 % SRB

solution in 1 % acetic acid for 15 min at RT. The excess of SRB stain was removed and the plates were washed with a 1 % acetic acid solution and let dry at RT. The SRB staining was dissolved in 150 μL of tris(hydroxymethyl)aminomethane solution pH = 8.8 (TRIS base), and the absorbance was measured at wavelengths of 490 nm and 540 nm. Cell growth inhibition was calculated as the percentage of drug treated cells versus vehicle-treated cells ("untreated cells or control") OD (corrected for OD before drug addiction, "day-0"). The comparison of the average optical density of the growth in control wells with that in the sample wells allowed estimating the percentage of cell growth, using the following equation:

$$\%\ Cell\ Growth = [(\text{mean ODcompound} - \text{mean ODday zero plate})/\text{mean (ODcontrol cells} - \text{mean ODday zero plate})] \times 100$$

The results obtained were adjusted by the day zero plate (wells containing cells growing for only 24 h) and normalized by the control cells (wells with untreated cells) to obtain the rate of viable cells. The 50 % inhibitory concentration of cell growth (IC_{50}) was calculated by non-linear least squares curve fitting (GraphPad PRISM, Intuitive Software for Science, San Diego, CA). In the NCI protocol IC_{50} is named GI_{50} (50 % growth inhibitory concentration). Data was expressed as mean values ± SEM.

Initially, the cells were exposed to three different screening concentrations (0.1 μM, 1 μM, 10 μM) of each series of compounds for a duration of 72 h. Subsequently, the SRB assay was performed to determine the inhibition of cell proliferation by the most active compounds. To determine the IC_{50} values for each PDAC cell model, cells were treated with eight increasing concentrations (ranging from 0.1 μM to 20 μM) of compounds **9a, 10a, 14a** and **15b** for 72 h.

4.2.4. Wound-healing assay

The *in vitro* scratch wound-healing assay was carried out following previously established methods [36,37]. PATU-T, SUIT-2 and PANC-1 cells were seeded in 96-well flat-bottom plates at a density of 3×10^4 cells/well in a volume of 100 μL. After 24 h of pre-incubation at 37 °C, 5 % CO_2, and 95 % humidity, scratches of consistent width were created on the cell monolayers using a specialized multi-needle tool. Following the removal of detached cells by washing with phosphate-buffered saline, the control wells received only medium, while the experimental wells were supplemented with the compounds of interest. The wound confluence was monitored at specific time points (T = 0, 4, 8, 20, and 24 h after treatment) using phase-contrast microscopy integrated with the Leica DMI300B migration station and Universal Grab 6.3 software from Digital Cell Imaging Labs, Keerbergen, Belgium. Images were captured, and the wound closure was analyzed using the Scratch Assay 6.2 software from Digital Cell Imaging Labs.

4.2.5. Human phospho-kinase array

The cells were cultivated in 25 cm^2 flasks until they reached 80 % confluence at a temperature of 37 °C and a CO_2 concentration of 5 %. Subsequently, cells were treated with 5 times the IC_{50} concentration of **14a** (*i.e,* 6.6 μM), while the control cells had their medium replaced with fresh medium. The treatment duration was 2 h, after which the cells were detached, and 10^6 cells/ml were collected from each replicate. The human phospho-kinase array was performed according to manufactures' instructions. In brief, PDAC cells were lysed in the kit provided lysis buffer and the membranes were blocked in array buffer for 1 h at room temperature. Subsequently, 2.0 mL diluted cell lysate were added into membranes and incubated overnight at 4C, followed by continue incubation with detection antibody cocktail A or detection antibody cocktail B for 2 h at room temperature. Afterwards, membranes were incubated with array buffer containing diluted streptavidin–HRP for 30 min. Finally, each spot corresponding to the amount of phosphorylated protein bound was acquired using enhanced chemiluminescence (ECL) and quantitated using Image Lab Software.

4.2.6. Cell cycle analysis

Cell cycle stage was analyzed by flow cytometry. Cells were seeded in 6 wells plate (2.5×10^5 cells/well). After an overnight incubation at 37 °C, the cells were treated with the compounds **14a** at two concentrations (i.e. IC_{50} and $5\times$ IC_{50}), and incubated for 24 h. After treatment, the cells were harvested by trypsinization (0.3 ml/well of trypsine-EDTA), incubated until the cells were detached; cells were resuspended with 1.7 ml of medium and collected into FACS tubes. The samples were then centrifuged in order to get cells pellet (5 min at 1200 rpm). Finally, these pellets were fixed in ice-cold 70 % ethanol, washed twice with phosphate-buffered saline (20 mM sodium phosphate pH 7.4, 150 mM NaCl) and incubated for 30 min at 37 °C with 50 μl of RNase (100 μg/ml) followed by incubation with 200 μl of propidium iodide solution (PI, 50 μg/ml). The cycle analysis was performed on the FACS (Fluorescence Activated Cell Sorting) Calibur instrument, to evaluate the effects on the cell cycle distribution and cell viability.

4.2.7. Spheroids

PATU-T cells were grown in in CELLSTAR®96-well cell repellent U-bottom plates (Greiner Bio-One, Cat No. 650970, Kremsmünster, Austria). Cells were seeded at the density of 2.5×10^3 cells/well and the plate was centrifuged *at 1200 rpm,* for 5 min at RT to facilitate cell aggregation, finally cells were incubated at 37 °C, 5 % CO_2 for 72 h in order to allow spheroids formation. The experiment was performed as previously described [39,40].

After 72 h, spheroids formation was checked with pictures of each condition taken with an automated phase-contrast microscope DMI300B (Leica Microsystems, Eindhoven, Netherlands), and the subsequent pictures were taken every two days.

Afterwards, the culture medium was replaced with drug-free medium for the control, whereas testing group was treated with compound **14a** (at least 8 wells per condition). Compound **14a** was diluted at 6.6 μM ($5 \times$ IC_{50}, obtained with previous growth-inhibition assay). The treatment was repeated after four days, to ensure the availability of nutrients.

Pictures were analysed with Image J Software (U.S. National Institute of Health, Bethesda, Maryland, USA) to determine the area of the spheroids treated and compare it to the area of the untreated spheroids, as described previously [41].

The *in vitro* experiments were performed in triplicates and repeated at least twice. The results reported in the figures are expressed as mean values ± standard error of the mean (SEM). Statistical analyses were carried out by two-way ANOVA followed by Bonferroni's post-test (to adjust for multiple comparisons), using GraphPad-Prism version 9 (Intuitive Software for Science, San Diego, CA). All analyses were two-sided, and statistical significance was set at $P < 0.05$.

4.2.8. Analysis of phospho-akt by enzyme linked immunosorbent (ELISA) assay

To assess the modulation effect of compound **14a** on Akt protein activation, Akt phosphorylation at serine 473 (pS473Akt) was analyzed using AKT Colorimetric ELISA kits (Thermo Scientific, Rockford, IL, USA). The levels of pS473Akt were quantified in PATU-T and SUIT-2 cells seeded in 96-well plates at a density of 1×10^5 cells per well, treated with the compound at its IC_{50} concentration for 2 h. Absorbance was measured at 450 nm using a microplate reader, following previously established protocols [42].

4.2.9. Analysis of apoptosis induction

PATU-T and SUIT-2 cells were exposed to compound **14a** at IC_{50} levels for 72 h. Following incubation, cells were rinsed twice with PBS and fixed in 4 % buffered paraformaldehyde (PFA) for 15 min. After resuspension, cells were incubated for another 15 min in a Hoechst-33258/bisbenzimide HCl solution (8 μg/ml). Drops of the cell suspension were then applied to glass slides and examined using fluorescence microscopy (Leica, Wetzlar, Germany). Two hundred cells were counted

in random fields, and the apoptotic index was calculated as the percentage of cells exhibiting chromatin condensation and nuclear fragmentation relative to the total cell count, as previously described [43].

CRediT authorship contribution statement

Camilla Pecoraro: Writing – review & editing, Data curation. **Fabio Scianò:** Data curation. **Daniela Carbone:** Formal analysis, Data curation. **Geng Xu:** Investigation, Formal analysis. **Juan Deng:** Formal analysis, Data curation. **Stella Cascioferro:** Writing – original draft, Data curation, Conceptualization. **Elisa Giovannetti:** Writing – review & editing, Conceptualization. **Patrizia Diana:** Writing – review & editing, Supervision, Conceptualization. **Barbara Parrino:** Writing – review & editing, Data curation, Conceptualization.

Declaration of competing interest

The authors declare that they have no known competing financial interests or personal relationships that could have appeared to influence the work reported in this paper.

Acknowledgement

This work was supported by KWF Dutch Cancer Society grants (#13598 and 15305)

Appendix A. Supplementary material

Supplementary data to this article can be found online at https://doi.org/10.1016/j.bioorg.2024.107959.

Data availability

No data was used for the research described in the article.

References

[1] E.M. Sale, G.J. Sale, Protein kinase B: signalling roles and therapeutic targeting, Cell. Mol. Life Sci. 65 (2008) 113–127, https://doi.org/10.1007/s00018-007-7274-9.
[2] M. Mortazavi, F. Moosavi, M. Martini, E. Giovannetti, O. Firuzi, Prospects of targeting PI3K/AKT/mTOR pathway in pancreatic cancer, Crit. Rev. Oncol. Hematol. 176 (2022) 103749, https://doi.org/10.1016/j.critrevonc.2022.103749.
[3] Y. Brand, S. Levano, V. Radojevic, A.M. Naldi, C. Setz, A.F. Ryan, K. Pak, B. A. Hemmings, D. Bodmer, All Akt isoforms (Akt1, Akt2, Akt3) are involved in normal hearing, but only Akt2 and Akt3 are involved in auditory hair cell survival in the mammalian inner ear, PLoS One 10 (2015) e0121599, https://doi.org/10.1371/journal.pone.0121599.
[4] G. Song, G. Ouyang, S. Bao, The activation of Akt/PKB signaling pathway and cell survival, J. Cell Mol. Med. 9 (2005) 59–71, https://doi.org/10.1111/j.1582-4934.2005.tb00337.x.
[5] N.M. Conus, K.M. Hannan, B.E. Cristiano, B.A. Hemmings, R.B. Pearson, Direct identification of tyrosine 474 as a regulatory phosphorylation site for the Akt protein kinase, J. Biol. Chem. 277 (2002) 38021–38028, https://doi.org/10.1074/jbc.M203387200.
[6] Y.O. Al-Bazz, J.C.E. Underwood, B.L. Brown, P.R.M. Dobson, Prognostic significance of Akt, phospho-Akt and BAD expression in primary breast cancer, Eur. J. Cancer 45 (2009) 694–704, https://doi.org/10.1016/j.ejca.2008.11.044.
[7] S.H. Sahlberg, A.C. Mortensen, J. Haglöf, M.K.R. Engskog, T. Arvidsson, C. Pettersson, B. Glimelius, B. Stenerlöw, M. Nestor, Different functions of AKT1 and AKT2 in molecular pathways, cell migration and metabolism in colon cancer cells, Int. J. Oncol. 50 (2016) 5–14, https://doi.org/10.3892/ijo.2016.3771.
[8] B. Dummler, B.A. Hemmings, Physiological roles of PKB/Akt isoforms in development and disease, Biochem. Soc. Trans. 35 (2007) 231–235, https://doi.org/10.1042/BST0350231.
[9] Y. He, M.M. Sun, G.G. Zhang, J. Yang, K.S. Chen, W.W. Xu, B. Li, Targeting PI3K/Akt signal transduction for cancer therapy, Sig. Transduct. Target. Ther. 6 (2021) 1–17, https://doi.org/10.1038/s41392-021-00828-5.
[10] D.S. Mortensen, S.M. Perrin-Ninkovic, G. Shevlin, J. Elsner, J. Zhao, B. Whitefield, L. Tehrani, J. Sapienza, J.R. Riggs, J.S. Parnes, P. Papa, G. Packard, B.G.S. Lee, R. Harris, M. Correa, S. Bahmanyar, S.J. Richardson, S.X. Peng, J. Leisten, G. Khambatta, M. Hickman, J.C. Gamez, R.R. Bisonette, J. Apuy, B.E. Cathers, S. S. Canan, M.F. Moghaddam, H.K. Raymon, P. Worland, R.K. Narla, K.E. Fultz, S. Sankar, Optimization of a series of triazole containing mammalian target of rapamycin (mTOR) kinase inhibitors and the discovery of CC-115, J. Med. Chem. 58 (2015) 5599–5608, https://doi.org/10.1021/acs.jmedchem.5b00627.
[11] I. Vivanco, C.L. Sawyers, The phosphatidylinositol 3-Kinase–AKT pathway in human cancer, Nat. Rev. Cancer 2 (2002) 489–501, https://doi.org/10.1038/nrc839.
[12] J. Karar, A. Maity, PI3K/AKT/mTOR pathway in angiogenesis, Front. Mol. Neurosci. 4 (2011) 51, https://doi.org/10.3389/fnmol.2011.00051.
[13] M. Song, A.M. Bode, Z. Dong, M.-H. Lee, AKT as a therapeutic target for cancer, Cancer Res. 79 (2019) 1019–1031, https://doi.org/10.1158/0008-5472.CAN-18-2738.
[14] D.T. Trafalis, S. Sagredou, P. Dalezis, M. Voura, S. Fountoulaki, N. Nikoleousakos, K. Almpanakis, M.V. Deligiorgi, V. Sarli, Anticancer activity of triazolo-thiadiazole derivatives and inhibition of AKT1 and AKT2 activation, Pharmaceutics 13 (2021) 493, https://doi.org/10.3390/pharmaceutics13040493.
[15] Y. Kommagalla, S. Cornea, R. Riehle, V. Torchilin, A. Degterev, C.V. Ramana, Optimization of the anti-cancer activity of the phosphatidylinositol-3 kinase pathway inhibitor PITENIN-1: switching thiourea with 1,2,3-triazole, Med. Chem. Commun. 5 (2014) 1359–1363, https://doi.org/10.1039/C4MD00109E.
[16] W.-J. Leu, S.P. Swain, S.-H. Chan, J.-L. Hsu, S.-P. Liu, M.-L. Chan, C.-C. Yu, L.-C. Hsu, Y.-L. Chou, W.-L. Chang, D.-R. Hou, J.-H. Guh, Non-immunosuppressive triazole-based small molecule induces anticancer activity against human hormone-refractory prostate cancers: the role in inhibition of PI3K/AKT/mTOR and c-Myc signaling pathways, Oncotarget 7 (2016) 76995–77009. 10.18632/oncotarget.12765.
[17] J.M. Hermanowicz, A. Szymanowska, B. Sieklucka, R. Czarnomysy, K. Pawlak, A. Bielawska, K. Bielawski, J. Kalafut, A. Przybyszewska, A. Surazynski, A. Rivero-Muller, M. Mojzych, D. Pawlak, Exploration of novel heterofused 1,2,4-triazine derivative in colorectal cancer, J. Enzyme Inhib. Med. Chem. 36 (2021) 535–548, https://doi.org/10.1080/14756366.2021.1879803.
[18] M. Kciuk, S. Mujwar, A. Szymanowska, B. Marciniak, K. Bukowski, M. Mojzych, R. Kontek, Preparation of novel pyrazolo[4,3-e]tetrazolo[1,5-b][1,2,4]triazine sulfonamides and their experimental and computational biological studies, Int. J. Mol. Sci. 23 (2022) 5892, https://doi.org/10.3390/ijms23115892.
[19] K.D. Freeman-Cook, C. Autry, G. Borzillo, D. Gordon, E. Barbacci-Tobin, V. Bernardo, D. Briere, T. Clark, M. Corbett, J. Jakubczak, S. Kakar, E. Knauth, B. Lippa, M.J. Luzzio, G. Mahmoud Mansour, M. Martinelli, K. Marx, J. Nelson, F. Pandit, S. Rajamohan, C. Robinson, L. Subramanyam, M. Wythes, Wei, J. Morris, Design of selective, ATP-competitive inhibitors of Akt, J. Med. Chem. 53 (2010) 4615–4622, https://doi.org/10.1021/jm1003842.
[20] B.R. Davies, H. Greenwood, P. Dudley, C. Crafter, D.-H. Yu, J. Zhang, J. Li, B. Gao, Q. Ji, J. Maynard, S.-A. Ricketts, D. Cross, S. Cosulich, C.C. Chresta, K. Page, J. Yates, C. Lane, R. Watson, R. Luke, D. Ogilvie, M. Pass, Preclinical pharmacology of AZD5363, an inhibitor of AKT: pharmacodynamics, antitumor activity, and correlation of monotherapy activity with genetic background, Mol. Cancer Ther. 11 (2012) 873–887, https://doi.org/10.1158/1535-7163.MCT-11-0824-T.
[21] M.G. Schlieman, B.N. Fahy, R. Ramsamooj, L. Beckett, R.J. Bold, Incidence, mechanism and prognostic value of activated AKT in pancreas cancer, Br. J. Cancer 89 (2003) 2110–2115, https://doi.org/10.1038/sj.bjc.6601396.
[22] S. Ebrahimi, M. Hosseini, S. Shahidsales, M. Maftouh, G.A. Ferns, M. Ghayour-Mobarhan, S. Mahdi Hassanian, A. Avan, Targeting the Akt/PI3K signaling pathway as a potential therapeutic strategy for the treatment of pancreatic cancer, Curr. Med. Chem. 24 (2017) 1321–1331, https://doi.org/10.2174/0929867324666170206142658.
[23] S. Cascioferro, G. Li Petri, B. Parrino, B. El Hassouni, D. Carbone, V. Arizza, U. Perricone, A. Padova, N. Funel, G.J. Peters, G. Cirrincione, E. Giovannetti, P. Diana, 3-(6-Phenylimidazo [2,1-b][1,3,4]thiadiazol-2-yl)-1H-indole derivatives as new anticancer agents in the treatment of pancreatic ductal adenocarcinoma, Molecules 25 (2020) 329, https://doi.org/10.3390/molecules25020329.
[24] D. Carbone, C. Pecoraro, G. Panzeca, G. Xu, M.S.F. Roeten, S. Cascioferro, E. Giovannetti, P. Diana, B. Parrino, 1,3,4-Oxadiazole and 1,3,4-thiadiazole nortopsentin derivatives against pancreatic ductal adenocarcinoma: synthesis, cytotoxic activity, and inhibition of CDK1, Drugs 21 (2023) 412, https://doi.org/10.3390/md21070412.
[25] D. Carbone, M. De Franco, C. Pecoraro, D. Bassani, M. Pavan, S. Cascioferro, B. Parrino, G. Cirrincione, S. Dall'Acqua, S. Sut, S. Moro, V. Gandin, P. Diana, Structural manipulations of marine natural products inspire a new library of 3-amino-1,2,4-triazine PDK inhibitors endowed with antitumor activity in pancreatic ductal adenocarcinoma, Mar. Drugs 21 (2023) 288, https://doi.org/10.3390/md21050288.
[26] D. Carbone, M. De Franco, C. Pecoraro, D. Bassani, M. Pavan, S. Cascioferro, B. Parrino, G. Cirrincione, S. Dall'Acqua, S. Moro, V. Gandin, P. Diana, Discovery of the 3-amino-1,2,4-triazine-based library as selective PDK1 inhibitors with therapeutic potential in highly aggressive pancreatic ductal adenocarcinoma, Int. J. Mol. Sci. 24 (2023) 3679, https://doi.org/10.3390/ijms24043679.
[27] C. Pecoraro, B. Parrino, S. Cascioferro, A. Puerta, A. Avan, G.J. Peters, P. Diana, E. Giovannetti, D. Carbone, A new oxadiazole-based topsentin derivative modulates cyclin-dependent kinase 1 expression and exerts cytotoxic effects on pancreatic cancer cells, Molecules 27 (2022) 19, https://doi.org/10.3390/molecules27010019.
[28] C. Pecoraro, D. Carbone, F. Scianò, F. Terrana, G. Xu, C. Bergonzini, M.S.F. Roeten, S. Cascioferro, G. Cirrincione, G. Cirrincione, P. Diana, E. Giovannetti, B. Parrino, Exploring the therapeutic potential of a novel series of imidazothiadiazoles targeting focal adhesion kinase (FAK) for pancreatic cancer treatment: synthesis, mechanistic insights and promising antitumor and safety profile, J. Drug Target. (2024) 1–17, https://doi.org/10.1080/1061186X.2024.2385557.
[29] G. Li Petri, B. El Hassouni, R. Sciarrillo, N. Funel, G. Mantini, E.A. Zeeuw van der Laan, S. Cascioferro, A. Avan, P.A. Zucali, N. Zaffaroni, T. Lagerweij, B. Parrino, K. Smid, M. Deraco, C. Granchi, A. Braczko, R.T. Smolenski, L.H. Matherly,

G. Jansen, Y.G. Assaraf, P. Diana, J. Cloos, G.J. Peters, F. Minutolo, E. Giovannetti, Impact of hypoxia on chemoresistance of mesothelioma mediated by the proton-coupled folate transporter, and preclinical activity of new anti-LDH-A compounds, Br. J. Cancer 123 (2020) 644–656, https://doi.org/10.1038/s41416-020-0912-9.

[30] L. Wu, X. Wang, Y. Chen, Q. Huang, Q. Lin, M. Wu, 4-Aryl-NH-1,2,3-triazoles via multicomponent reaction of aldehydes, nitroalkanes, and sodium azide, Synlett 27 (2015) 437–441, https://doi.org/10.1055/s-0035-1560528.

[31] C. Bergonzini, A. Gregori, T.M.S. Hagens, V.E. van der Noord, B. van de Water, A.J. M. Zweemer, B. Coban, M. Capula, G. Mantini, A. Botto, F. Finamore, I. Garajova, L.A. McDonnell, T. Schmidt, E. Giovannetti, E.H.J. Danen, ABCB1 overexpression through locus amplification represents an actionable target to combat paclitaxel resistance in pancreatic cancer cells, J. Exp. Clin. Cancer Res. 43 (1) (2024) 4, https://doi.org/10.1186/s13046-023-02879-8.

[32] M. Shariati, F. Meric-Bernstam, Targeting AKT for cancer therapy, Expert Opin. Invest. Drugs 28 (2019) 977–988, https://doi.org/10.1080/13543784.2019.1676726.

[33] S. Stanciu, F. Ionita-Radu, C. Stefani, D. Miricescu, I.-I. Stanescu-Spinu, M. Greabu, A. Ripszky Totan, M. Jinga, Targeting PI3K/AKT/mTOR signaling pathway in pancreatic cancer: from molecular to clinical aspects, Int. J. Mol. Sci. 23 (2022) 10132, https://doi.org/10.3390/ijms231710132.

[34] H.W. Yung, D.S. Charnock-Jones, G.J. Burton, Regulation of AKT phosphorylation at Ser473 and Thr308 by endoplasmic reticulum stress modulates substrate specificity in a severity dependent manner, PLoS One 6 (2011) e17894, https://doi.org/10.1371/journal.pone.0017894.

[35] G. Xiao, Y. Li, X. Qiang, R. Xu, Y. Zheng, Z. Cao, L. Luo, X. Yang, Z. Sang, F. Su, Y. Deng, Design, synthesis and biological evaluation of 4′-aminochalcone-rivastigmine hybrids as multifunctional agents for the treatment of Alzheimer's disease, Bioorg. Med. Chem. 25 (2017) 1030–1041, https://doi.org/10.1016/j.bmc.2016.12.013.

[36] WO2015179559 A2, Pyrazole compounds as modulators of MAGL, ABHD6 and FAAH and methods of making and using same, 2015-11-26.

[37] B. Zhang, J. Zeng, Y. Yan, B. Yang, M. Huang, L. Wang, Q. Zhang, N. Lin, Ethyl acetate extract from Inula helenium L. inhibits the proliferation of pancreatic cancer cells by regulating the STAT3/AKT pathway, Mol. Med. Rep. 17 (2018) 5440–5448, https://doi.org/10.3892/mmr.2018.8534.

[38] R.E. Dolle, B. Le Bourdonnec, G.-H. Chu, Spirocyclic heterocyclic derivatives and methods of their use, WO2006105442 A2, 2006.

[39] D. Carbone, C. Pecoraro, G. Panzeca, G. Xu, M.S.F. Roeten, S. Cascioferro, E. Giovannetti, P. Diana, B. Parrino, 1,3,4-Oxadiazole and 1,3,4-thiadiazole nortopsentin derivatives against pancreatic ductal adenocarcinoma: synthesis, cytotoxic activity, and inhibition of CDK1, Mar. Drugs 21 (2023) 412, https://doi.org/10.3390/md21070412.

[40] M. Maftouh, A. Avan, N. Funel, A.E. Frampton, H. Fiuji, S. Pelliccioni, L. Castellano, V. Galla, G.J. Peters, E. Giovannetti, miR-211 modulates gemcitabine activity through downregulation of ribonucleotide reductase and inhibits the invasive behavior of pancreatic cancer cells, Nucleosides Nucleotides Nucleic Acids 33 (2014) 384–393, https://doi.org/10.1080/15257770.2014.891741.

[41] R. Sciarrillo, A. Wojtuszkiewicz, B.E. Hassouni, N. Funel, P. Gandellini, T. Lagerweij, S. Buonamici, M. Blijlevens, E.A.Z. van der Laan, N. Zaffaroni, M. Deraco, S. Kusamura, T. Würdinger, G.J. Peters, C.F.M. Molthoff, G. Jansen, G.J. L. Kaspers, J. Cloos, E. Giovannetti, Splicing modulation as novel therapeutic strategy against diffuse malignant peritoneal mesothelioma, eBioMedicine 39 (2019) 215–225, https://doi.org/10.1016/j.ebiom.2018.12.025.

[42] D. Massihnia, A. Avan, N. Funel, M. Maftouh, A. van Krieken, C. Granchi, R. Raktoe, U. Boggi, B. Aicher, F. Minutolo, A. Russo, L.G. Leon, G.J. Peters, E. Giovannetti, Phospho-Akt overexpression is prognostic and can be used to tailor the synergistic interaction of Akt inhibitors with gemcitabine in pancreatic cancer, J. Hematol. Oncol. 10 (1) (2017) 9, https://doi.org/10.1186/s13045-016-0371-1.

[43] A. Gregori, C. Bergonzini, M. Capula, G. Mantini, F. Khojasteh-Leylakoohi, A. Comandatore, G. Khalili-Tanha, A. Khooei, L. Morelli, A. Avan, E.H. Danen, T. Schmidt, E. Giovannetti, Prognostic significance of integrin subunit alpha 2 (ITGA2) and role of mechanical cues in resistance to gemcitabine in pancreatic ductal adenocarcinoma (PDAC), Cancers (Basel) 15 (3) (2023) 628, https://doi.org/10.3390/cancers15030628.